Ultra-Peripheral Collisions with STAR at RHIC

Spencer Klein[a], for the STAR collaboration

[a]Lawrence Berkeley National Laboratory, Berkeley, CA 94720

The strong electromagnetic fields of heavy nuclei can produce a wide variety of two-photon and photonuclear reactions at relativistic ion colliders. We present recent results from the STAR collaboration on these 'ultra-peripheral' interactions, focusing on vector meson production and interferometry, and on e^+e^- pair production. The vector meson interferometry occurs because of the symmetric initial state: nucleus 1 can emit a photon which scatters from nucleus 2, emerging as a vector meson, or vice-versa. The two processes are indistinguishable, and so interfere, even though the production points are separated enough that the produced mesons decay before their wave functions can overlap, so the system can be used for interesting tests of quantum mechanics.

1. Introduction

Electromagnetic interactions between relativistic heavy ions occur frequently, even at impact parameters b large enough that no hadronic interactions occur [1]. The electromagnetic fields may be treated as fields of almost-real photons, following the Weizsäcker-Williams method; the photon flux scales as Z^2, so the cross sections are large.

These ultra-peripheral collisions (UPCs) can be divided into two classes, purely electromagnetic interactions (two-photon) and photonuclear interactions, where a photon from the field of one nucleus interacts with the other nucleus. We focus on the region $b > 2R_A$ to exclude hadronic contamination. We will present 3 topics which have been studied by the Solenoidal Tracker at RHIC (STAR) collaboration: vector meson production, vector meson interferometry, and e^+e^- pair production.

Vector mesons are produced when a photon from the field of one nucleus fluctuates to a $q\overline{q}$ pair (virtual vector meson), which then scatters elastically from the other nucleus, emerging as a vector meson [2], as is shown in Fig. 1a. The elastic scattering is colorless, and can be described in terms of Pomeron exchange. For light mesons like the ρ^0, the cross section rises slowly with the photon energy k. For small momentum transfers, the elastic scattering is coherent over the entire nuclear target. In the coherent region, the cross section depends on the size of the $q\overline{q}$ dipole fluctuation.

Heavy mesons come from small dipoles with small interaction cross sections. Production is distributed evenly throughout the target, and $\sigma \approx A^2$. For sufficiently heavy mesons like the J/ψ, the elastic scattering may be described in terms of multiple gluon exchange. The cross section is sensitive to gluon shadowing in nuclei [3].

Large dipoles (light mesons) interact with a large cross section with the first nucleon that they encounter. The interaction is on the surface of the target, so $\sigma \approx A^{4/3}$. The exact scaling can be determined by a Glauber calculation [4,5]; for the ρ^0, the scaling is roughly $A^{5/3}$.

The large photon flux and the coherent scattering lead to a large cross section for ρ^0 production. For 200 GeV per nucleon Au-Au collisions at RHIC, the cross section for ρ^0 production is 590 mb, or about 8% of the hadronic cross section [4]. The STAR collaboration has already published results on ρ^0 production in Au-Au collisions at an energy of 130 GeV per nucleon [6]. The cross sections agreed with the Glauber calculations.

The elastic scattering involves the strong force, and so has a very short range [7]. The ρ production is localized to within 1 fm of the two ions. There are two possibilities: either nucleus 1 emits a photon which scatters off nucleus 2, or vice versa. These two possibilities are indistinguish-

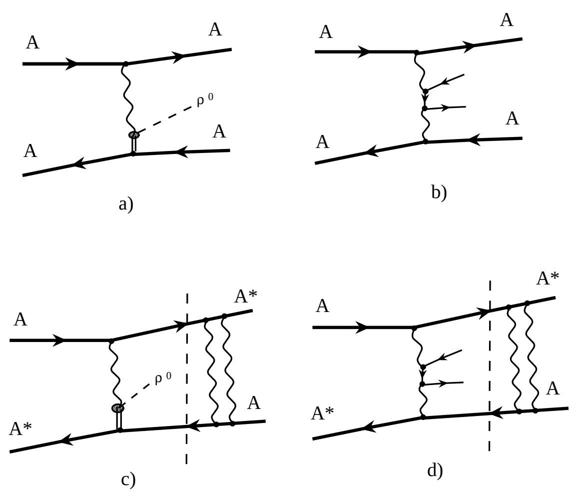

Figure 1. Schematic diagrams for (a) ρ^0 production and (b) e^+e^- production. These processes may be accompanied by mutual Coulomb excitation, as in (c) and (d) respectively. The dashed lines in (c) and (d) show the factorization, Eq. 3.

able, and are related by a parity tranformation. Vector mesons have negative parity, so the two amplitudes subtract, with a transverse momentum (p_T) dependent phase factor to account for the separation. The cross section is [8]

$$\sigma = \left|A_1 - A_2 \exp\left(ip_T \cdot b\right)\right|^2 \tag{1}$$

where A_1 and A_2 are the amplitudes for ρ^0 production from the two directions. At mid-rapidity $A_1 = A_2$ and this simplifies to

$$\sigma = \sigma_0\big[(1 - \cos\left(p_T \cdot b\right)\big] \tag{2}$$

where σ_0 is the cross section without interference. The system acts as a 2-slit interferometer, with slit separation b [9]. Of course, b is unmeasurable, and the observed p_T spectrum is obtained by integrating Eq. (1) over b. The p_T spectrum is suppressed for $p_T < \hbar/\langle b\rangle$, where $\langle b\rangle$ is the median impact parameter.

The ρ decay distance, $\gamma\beta c\tau < 1$ fm is far less than $\langle b\rangle \approx 46$ fm. The ρ^0 decay before the two amplitudes can overlap, making this an interesting test of quantum mechanics [10].

Two-photon processes like e^+e^-, Fig. 1b production are purely electromagnetic. To lowest order, it involves 2 photons, so the cross section scales as Z^4. At RHIC, the cross section is expected to be huge - 33,000 barns for gold beams. The coupling constant $Z\alpha \approx 0.6$ is large, so perturbative descriptions of this process may not be adequate. The calculated Coulomb corrections to the lowest order diagram reduce the cross section by 25% [11]. However, recent all-orders calculations find a cross section that matches the lowest order result [12]. The apparent discrepancy is not well understood [13].

In UPCs, the coupling constant $Z\alpha$ (where $\alpha \approx 1/137$ is the electromagnetic coupling constant) is very large, so multiple interactions between a single ion pair are common. ρ^0 or e^+e^- production may be accompanied by mutual Coulomb excitation, as in Figs. 1c and 1d. Each ion emits a photon, which excites the other nucleus, usually to a giant dipole resonance (GDR). The excited nucleus decays by emitting one or more neutrons. These neutrons serve as a distinctive experimental signature of nuclear dissociation. The presence of mutual Coulomb dissociation can be used to 'tag' collisions at moderate impact parameters, $2R_A < b <\approx 30$ fm [14]. Except for the shared impact parameter, the reactions are independent [15]. For example, the cross section for ρ^0 production with mutual Coulomb dissociation is

$$\sigma = \int d^2b P_\rho(b) P_{2EXC}(b)[1 - P_{had}(b)] \tag{3}$$

where $P_\rho(b)$ and $P_{2EXC}(b)$ are the probabilities for ρ^0 production and mutual excitation respectively. Here, $P_{had}(b)$ is the probability of having a hadronic interaction; the last term has an effect similar to setting a minimum impact parameter $b_{min} = 2R_A$. For gold ions, $P_\rho(2R_A) \approx 1\%$ and $P_{2EXC}(2R_A) \approx 30\%$, so the probability of multiple interactions is substantial. The multiple photon exchange skews these interactions to smaller b. This leads to a harder photon spectrum, and as can be seen from Eq. (2), interference at larger p_T.

2. The STAR Detector

The STAR detector studies heavy ion and polarized proton collisions at the Relativistic Heavy Ion Collider (RHIC) at Brookhaven National Laboratory. STAR is optimized to study central heavy ion collisions, which may contain thousands of particles [16]. However, it is also quite effective for studying UPCs where the final states contain 2-4 particles. STAR has collected UPC data in gold-gold collisions at energies of 130 GeV per nucleon (in 2000) and 200 GeV per nucleon (in 2001). STAR has also studied ρ^0 photoproduction in 200 GeV per nucleon deuteron on gold collisions [17]. In dA collisions, the photon usually comes from the gold nucleus, removing the photon direction ambiguity present in the gold-gold collisions. This writeup will focus on the 200 GeV per nucleon gold-gold collisions.

Charged particles are reconstructed in a 4.2 meter long, 4 meter diameter time projection chamber (TPC) [18]. The TPC is in a solenoidal magnetic field which has been operated at both 0.25 and 0.5 T. At 0.5 T, the reconstruction efficiency for charged pions is high for tracks with transverse momentum $p_T > 100$ MeV/c and pseudorapidity $|\eta| < 1.15$. The track position and specific energy loss, dE/dx were measured at 45 points for high momentum charged particles with $|\eta| < 1$. In a 0.5 T field, the dE/dx resolution was 8%. The TPC is surrounded by 240 scintillator slats covering $|\eta| < 1$, comprising the central trigger barrel (CTB). Two zero degree calorimeters (ZDCs) are located 18 m upstream and downstream of the interaction point. These calorimeters are sensitive to neutrons from mutual Coulomb dissociation [19].

Two different triggers [20] were used to study UPCs. The 'topology' trigger selected events with an appropriate topology in the CTB. It divided the CTB into 4 quadrants: north, south, top and bottom, and required hits in the north and south quadrants. The top and bottom regions were used as vetoes to reject cosmic rays.

The minimum bias trigger selected events with one or more neutrons in each ZDC. The ZDC signals were required to occur within 1 nsec, restricting these events to the central 30 cm of the TPC. Data from both triggers was processed identically, except that events from the CTB based trigger were distributed more broadly along the TPC axis, and consequently, were accepted in a broader range.

3. ρ^0 Production

UPC ρ^0 production has a distinctive signature - two oppositely charged tracks with small net p_T. We select events with exactly 2 primary tracks that form a vertex. The vertexing procedure considers all of the tracks in an event, and rejects tracks that are inconsistent with coming from a single vertex. We do allow a few non-primary background tracks in the TPC. The topology and minimum bias data were treated identically, except that allowance was made for the different distribution of the accepted event production points. This study used about 1.5 million minimum bias and about 1.7 million topology triggers taken in a 0.5 T field for 200 GeV per nucleon interactions.

Figure 2a shows the p_T distribution of all charge-0 2-track vertices. The large peak for $p_T < 100$ MeV/c is a signature of fully coherent interactions. Like-sign pion pairs (the shaded histogram) are used as a background estimate; they are normalized to fit the unlike-sign pairs for $p_T > 250$ MeV/c. This procedure treats incoherent ρ^0 production (a photon scattering from a single nucleon in the target) as background.

Figure 2b shows the rapidity distribution of the coherent ρ^0 (pairs with $p_T < 150$ MeV/c). The points (data) are in excellent agreement with a calculation based on the soft Pomeron model and our detector simulation.

Figure 2c shows the $\pi\pi$ invariant mass, $M_{\pi\pi}$ for the sample. The data is fit to a relativistic Breit-Wigner for the ρ^0, plus a Söding term to account for the interference with direct $\pi^+\pi^-$ production[21]. The interference shifts the peak of the distribution to lower $M_{\pi\pi}$. The direct $\pi\pi$ to ρ ratio agrees with the STAR 130 GeV analysis [6] and with that observed by the ZEUS collaboration in γp interactions [22]. However, because of the coherent enhancement, the STAR data is at smaller $|t|$ than the ZEUS analysis, so the two results may not be directly comparable [23].

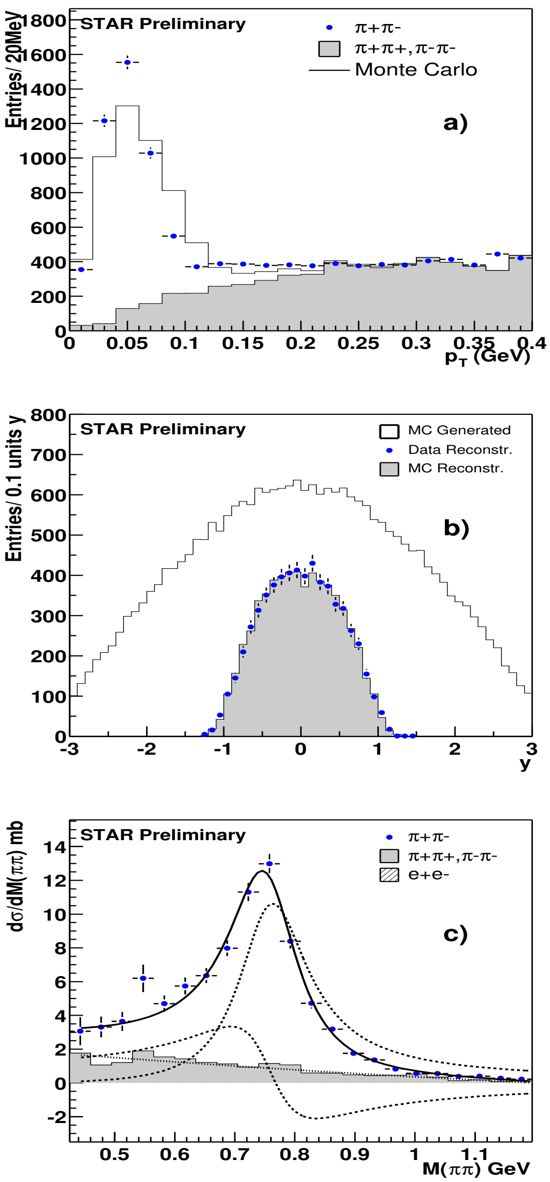

Figure 2. The (a) p_T, (b) rapidity and (c) $\pi\pi$ invariant mass spectra of ρ^0 using data from the minimum bias trigger. The mass is fit to to a Breit-Wigner function for the ρ^0, plus a Söding term due to interference with a direct $\pi\pi$ component. The combinatoric hadronic and coherent e^+e^- pair backgrounds are also shown.

4. ρ^0 Interferometry

For the interference analysis, a clean, low-background sample is important, so stringent event selection criteria were used, at some cost in efficiency. Events were required to have exactly two tracks with a vertex within 50 cm longitudinally of the center of the TPC for the minimum bias sample, and 100 cm for the topology sample. ρ^0 candidates were further required to have rapidity $|y| > 0.1$, to eliminate a small remaining cosmic ray contamination. Finally, the pairs were required to have 550 MeV $< M_{\pi\pi} <$ 920 MeV. The minimum mass cut removed most of the hadronic backgrounds, which are concentrated at low $M_{\pi\pi}$. These cuts reduced the like-sign pair background to a few percent. With these cuts, background from misidentified two-photon production of lepton pairs should be very small. The sample still includes direct pions, which should have the same spin/parity and quantum mechanical behavior as the pion pairs from ρ decay. We do not distinguish between the two sources.

The interference depends on the amplitudes for ρ production on the two nuclei. Away from $y = 0$, the photon energies for the two photon directions differ, $k_{1,2} = M_V/2\exp(\pm y/2)$; the amplitudes differ and the interference is less than maximal. Although it is not expected in the soft-Pomeron model, the the photon energy difference could introduce a small ρ^0 production phase difference, which could affect the interference [2]. This analysis focuses on the region near mid-rapidity where any phase difference is small. A Monte Carlo calculation is used to find the interference for different rapidity ranges [4,8].

We use the variable $t_\perp = p_T^2$ to study the interference. At RHIC energies, the longitudinal component of the 4-momentum transfer is small, so $t \approx t_\perp$. Without interference, the spectrum $dN/dt \approx \exp(-bt)$ for a variety of nuclear models [8,24]. Our calculations use a Woods-Saxon distribution for the gold density distribution.

Figure 3 compares the uncorrected minimum bias data for $0.1 < |\eta| < 0.5$ with two simulations, with and without interference. Both simulations include the detector response. The data has a significant downturn for $t < 0.001$ GeV^2, consis-

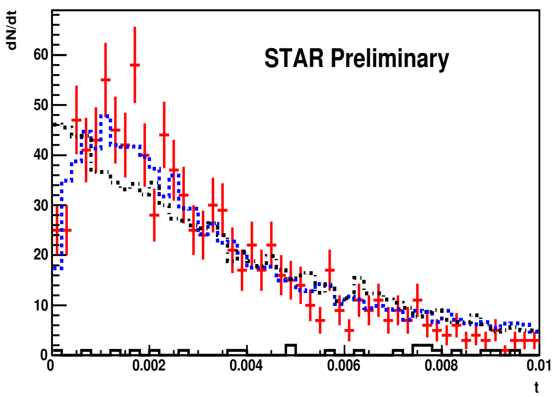

Figure 3. Raw (uncorrected) $t_\perp$ spectrum for ρ^0 sample for $0.1 < |y| < 0.5$ for the topology data. The points (red) are the data. The dashed histogram (blue) is a simulation that assumes that there is interference, while the dot-dash histogram (black) is based on a calculation without interference. The solid black histogram with very few counts is the like-sign background.

tent with the $\langle b \rangle = 20$ fm expected for a 3-photon reaction[15]. This drop matches the drop seen in the calculation with interference, but is absent in the calculation without the interference.

The efficiency corrected data are shown in Fig. 4. Minimum bias and topology data are shown separately, each with two rapidity bins: $0.1 < |y| < 0.5$ and $0.5 < |y| < 1.0$. The efficiency is independent of p_T. However p_T smearing (resolution) does affect the spectrum slightly. The ρ^0 p_T resolution is about 9 MeV/c, while the 1st t bin covers 0 to (15 MeV/c)^2. Interference depletes the first few bins, but feed down from the higher t bins partially repopulates them.

The data is fit to the 3-parameter form:

$$\frac{dN}{dt} = a\exp(-bt)[1 + c(R(t) - 1] \quad (4)$$

where $R(t) = Int(t)/Noint(t)$ is the ratio of the Monte Carlo t-spectra with and without interference. Here, a is the overall normalization, the slope $b \approx R_A^2$, and c is the degree of spectral modification; $c = 0$ corresponds to no interference while $c = 1$ is the expected interference. This functional form separates the interference (c) from the nuclear form factor (b).

Trigger	Rapidity	b (GeV^{-2})	c
M.B.	$0.1 - 0.5$	301 ± 14	1.01 ± 0.08
M.B.	$0.5 - 1.0$	304 ± 15	0.78 ± 0.13
Topo.	$0.1 - 0.5$	361 ± 10	0.71 ± 0.16
Topo.	$0.5 - 1.0$	368 ± 12	1.22 ± 0.21

Table 1
Results of the fits to the minimum bias (M.B.) and topology (topo.) data for two rapidity bins. The fits have χ^2 of 50, 73, 81 and 50 respectively for 47 degrees of freedom.

Table 1 gives the results of the fits. At small-rapidities the amplitudes from the two directions are similar and the interference reduces the cross section at $p_T = 0$ by more than at larger rapidities. In the minimum bias data, the interference extends to higher p_T than the topology data because the former has a smaller $\langle b \rangle$.

The 4 c values are consistent within errors; the weighted average is $c = 0.93 \pm 0.06$. The b values for the minimum bias and exclusive ρ^0 data differ by 20%: 364 ± 7 GeV^{-2} for the exclusive ρ versus 303 ± 10 GeV^{-2} for the Coulomb breakup events.

The different b values may be attributed to the different impact parameter distributions caused by the nuclear breakup tagging in the minimum bias data. The photon flux depends on the impact parameter as $1/b^2$. When $b \approx \text{few} R_A$, ρ are more likely to be produced on the side of the target near the photon emitter than on the far side. ρ^0 production is concentrated on the near side, leading to a smaller effective production volume and the smaller b. This near-side skewing affects the interference slightly, but is not included in current calculations.

Systematic errors come from a variety of sources. We have studied the effect of detector distortions (primarily p_T smearing) by turning off the detector simulation and comparing raw simulations with reconstructed data. This lowered c by 18%; if the detector simulation is 75% correct (a very conservative assumption), then detector effects are a less than 5% systematic un-

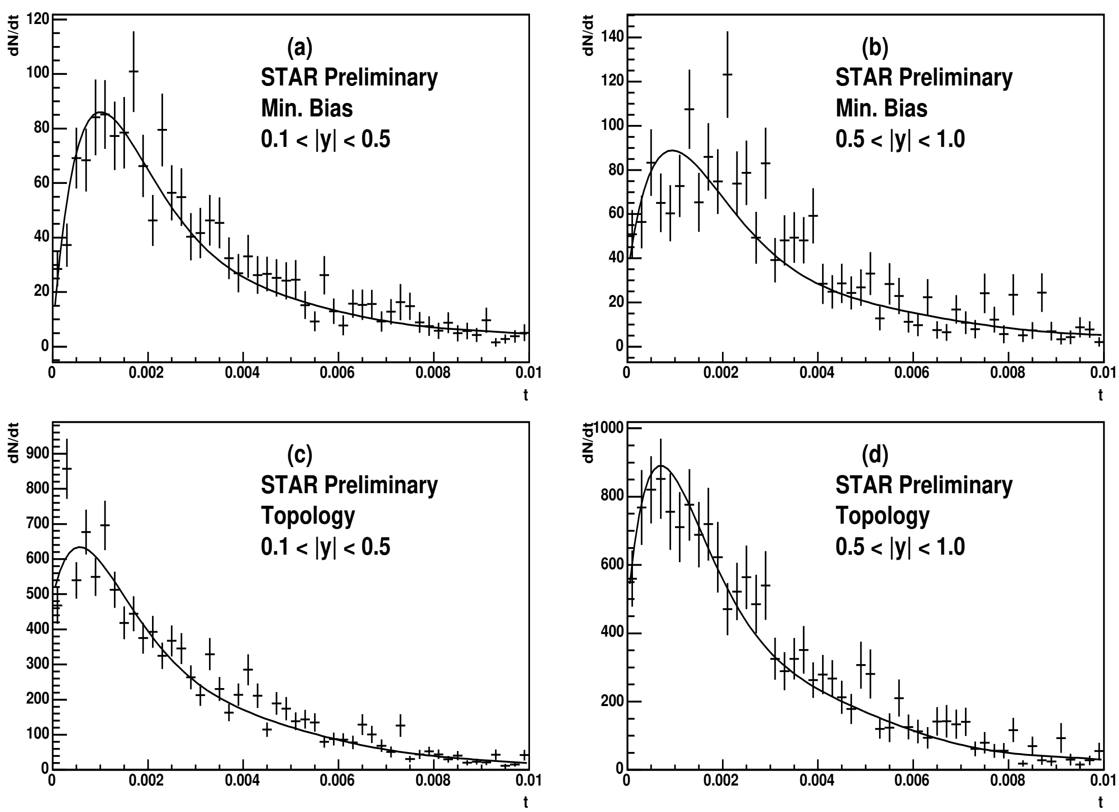

Figure 4. Efficiency corrected $t_{\perp}$ spectrum for ρ^0 from (a) mutual dissociation with $0.1 < |y| < 0.5$, (b) mutual dissociation with $0.5 < |y| < 1.0$, (c) topology trigger with $0.1 < |y| < 0.5$ and (d) topology trigger with $0.5 < |y| < 1.0$. The points are the data, while the solid line is the result of the fit to Eq. 4.

certainty. Minor systematic uncertainties come from backgrounds and the fitting procedure. We have compared the data and simulations for a variety of kinematic and detector-based variables, and found good agreement. We estimate a preliminary experimental systematic uncertainty of 8%.

This analysis depends on the shape of $R(t)$, which is calculated following Ref. [8]. For the broader picture, it is necessary to consider the simplifications in Ref. [8]. The calculation averages the photon flux over the surface of the nucleus, rather than incorporating the proper $1/b^2$ weighting. This may partly explain the relatively poor fit for the large-$|y|$ Coulomb breakup fit. We estimate that the effective impact parameter should be within 10% of the actual ion-ion separation for the coulomb breakup data, and 3% for the exclusive ρ. The uncertainties in the calculations should be at most a 15% effect. With this, the interference is $93\pm6(stat.)\pm8(syst.)\pm15(theory)\%$ (STAR preliminary) of that expected.

The ρ decays rapidly, with $\gamma\beta c\tau \ll \langle b\rangle$ and the two ρ decay points are well separated in space-time. In the usual space-time picture, the decays occur independently, and any interference must involve the final state $\pi^+\pi^-$. Interference must involve identical final states from the two sources. However, given the large available phase space for the decays, this is very unlikely for independent decays.

One possible interpretation of this result is given in Ref. [10]. In it, the interference occurs because the post-decay wave function includes amplitudes for all possible final states, then the amplitudes for identical states subtract, and the interference is visible. Because of the two sources, the $\pi^+\pi^-$ wave function is non-factorizable, and thus exhibits the Einstein-Podolsky-Rosen paradox [25]. We find that the decoherence, $1-c$, due to environmental or other factors is less than 43% at the 90% confidence level.

5. e^+e^- Pairs

The cross section for the production of e^+e^- pairs is peaked near threshold, with pair mass $M_{ee}\approx 3.5m$, where m is the electron mass. The pairs are produced predominantly in a forward-backward topology, with the $e^\pm$ produced with large longitudinal (along the beampipe) momentum and small p_T. This complicates experimental detection at an ion collider, and reduces the statistics available to any analysis. This analysis used data about 800,000 minimum bias triggers taken in a 0.25 T magnetic field. The lower magnetic field (compared to the 0.5 T full field data) increased the sensitivity to low p_T particles. The minimum bias trigger freed the electrons from the requirement that they have a high enough p_T to reach the CTB.

This analysis [26] used tracks with $p_T > 65$ MeV/c and pseudorapidity $|\eta| < 1.15$. In this region, tracking efficiency for electrons was above 80%. The electrons were identified by dE/dx. To get good electron/hadron separation, we required the tracks to have $p < 130$ MeV/c. In this momentum region, electrons had considerably higher dE/dx than hadrons, and the identification efficiency was nearly 100%, with minimal contamination. The cross section falls steeply with increasing M_{ee}, so few leptons were expected with higher momenta. We also required the events to have pair $p_T < 100$ MeV/c, pair rapidity $|y| < 1.15$ and pair mass 140 MeV $< M_{ee} <$ 265 MeV. These cuts selected a sample of 52 events.

The major backgrounds in this analysis are due to misidentified coherent $\pi^+\pi^-$ pairs and incoherent hadronic backgrounds. The former can be calculated from the known cross section and misidentification probability. The latter can be studied by using like sign ($\pi^+\pi^+$) pairs. The total background is estimated to be about 1.1 events.

The integrated luminosity of 94 ± 9 mb^{-1} was estimated by counting hadronic events with at least 8 tracks. This selected 80% of all hadronic gold-gold interactions. The integrated luminosity is based on an assumed gold-gold hadronic cross section of 7.2 barns.

Figure 5 shows the cross section as functions of pair mass and p_T. The data is compared with two calculations. The first, shown by the solid line, uses Eq. 3, with a equivalent photon calculation for $P_{ee}(b)$. The second, provided by Kai Hencken, was a quantum electrodynamic calculation, including photon virtuality. The major dif-

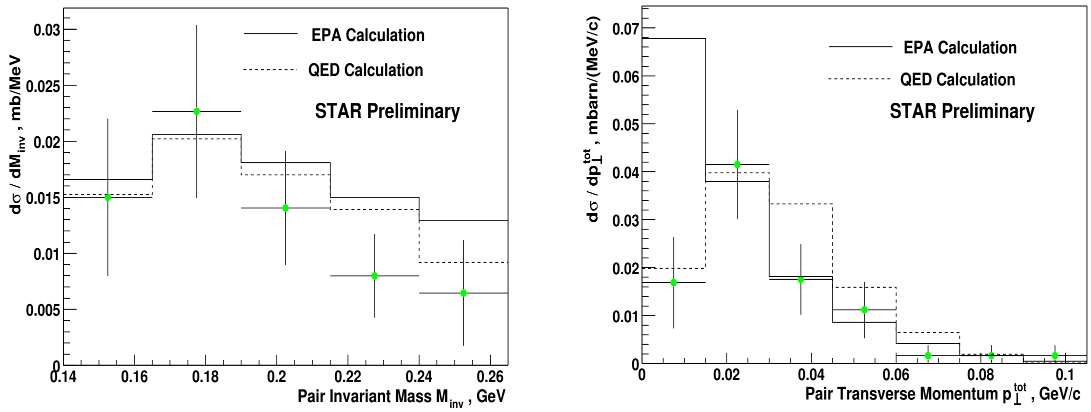

Figure 5. Differential Cross sections for pair (a) mass and (b) p_T. The data (points) are compared with the results of a equivalent photon calculation (solid) and a quantum electrodynamics calculation (dashed line). All data and calculations are restricted to the kinematic region described in the text.

ference between the results of the two calculations occurs for $p_T < 15$ MeV/c. The data strongly favors the QED calculation, by 4σ.

As expected, the $\langle p_T \rangle$ for e^+e^- production is smaller than for ρ^0 production. This is because the Pomeron p_T scale is roughly $\hbar/R_A$, while the photon p_T scale is very roughly $M_{ee}/\gamma \approx \hbar/b$.

Within the kinematic acceptance region, we find a cross section $\sigma = 1.6 \pm 0.2 \pm 0.3$ mb (STAR preliminary). The major systematic errors are due to tracking and vertexing uncertainty, and the integrated luminosity. This is 1.2σ lower than the equivalent photon prediction of 2.1 mb, and 0.8σ below the QED calculation of $\sigma_{QED} = 1.9$ mb for the same kinematic cuts. This measurement and the QED calculation can be used to put limits on possible higher order corrections $\Delta\sigma$ to the cross section. At a 90% confidence level, we find $-0.5\sigma_{QED} < \Delta\sigma < 0.2\sigma_{QED}$.

6. Conclusions

STAR has studied a number of photonuclear and two-photon reactions. We observe both exclusive ρ^0 production and ρ^0 production accompanied by nuclear excitation. The cross sections and rapidity distributions match the predictions of the soft Pomeron model. We observe destructive interference between the two production sites, at the expected level, and set an upper limit on decoherence. Finally, we observe e^+e^- pair production accompanied by mutual Coulomb dissociation. The kinematic distributions match those predicted by lowest order quantum electrodynamics.

We thank Tony Baltz for providing the calculations of nuclear breakup and Kai Hencken for providing the QED calculations. This work was supported by the U.S. DOE under contract number DE-AC-03-76SF00098.

REFERENCES

1. G. Baur *et al.*, Phys. Rep. **364**, 359 (2002); F. Krauss, M. Greiner and G. Soff, Prog. Part. Nucl. Phys. **39**, 503 (1997).
2. T. H. Baur *et al.*, Rev. Mod. Phys. **50**, 261 (1978).
3. L. Frankfurt, M. Strikman and M. Zhalov, Phys. Lett. **B540**, 220 (2002); L. Frankfurt *et al.*, JHEP **8**, 43 (2003).
4. S. Klein and J. Nystrand, Phys. Rev. **C60**, 014903 (1999).
5. L. Frankfurt, M. Strikman and M. Zhalov, Phys. Rev. **C67**, 034901 (2003).
6. C. Adler *et al.*, Phys. Rev. Lett. **89**, 272302

(2002).
7. B. Müller and A. J. Schramm, Nuclear Physics **A523**, 677 (1991).
8. S. Klein and J. Nystrand, Phys. Rev. Lett. **84**, 2330 (2000).
9. An analagous two-slit interferometer is described by T. Sudbery in *Quantum Concepts in Space and Time*, ed. R. Penrose and C. J. Isham, (Oxford, 1986).
10. S. Klein and J. Nystrand, Phys. Lett. **A308**, 323 (2003).
11. D. Yu Ivanov, A. Schiller and V. Serbo, Phys. Lett. **B454**, 155 (1999).
12. A. J. Baltz and L. D. McLerran, Phys. Rev. **C58**, 1679 (1998).
13. A. Aste *et al.*, Eur. Phys. J. **C23**, 545 (2002).
14. A. Baltz, S. Klein and J. Nystrand, Phys. Rev. Lett. **89**, 012301 (2002).
15. G. Baur *et al.*, nucl-th/0307031.
16. K. H. Ackermann *et al.*, Nucl. Instrum. & Meth. **A499**, 624 (2003).
17. F. Meissner and V. B. Morozov, nucl-ex/0307006 (2003).
18. M. Anderson *et al.*, Nucl. Instrum. & Meth. **A499**, 659 (2003); M. Anderson *et al.*, Nucl. Instrum. & Meth. **A499**, 679 (2003).
19. C. Adler *et al.*, Nucl. Instrum. & Meth. **A470**, 488 (2001).
20. F. S. Bieser *et al.*, Nucl. Instrum. & Meth. **A499**, 766 (2003).
21. P. Söding, Phys. Lett. **19**, 702 (1966).
22. J. Breitweg *et al.*, Eur. Phys. J. **C15**, 1 (2000).
23. Mark Strikman, private communication (2003).
24. M. Alvensleben *et al.*, Phys. Rev. Lett. **24**, 792 (1970).
25. A. Einstein, B. Podolsky and N. Rosen, Phys. Rev. **47**, 777 (1935).
26. V. Morozov, PhD Dissertation, UC Berkeley, 2003.